2022 IEEE/RSJ International Conference on Intelligent Robots and Systems (IROS)
October 23-27, 2022, Kyoto, Japan

Design of EMG-driven Musculoskeletal Model for Volitional Control of a Robotic Ankle Prosthesis

Chinmay Shah[1], Aaron Fleming[2], Varun Nalam[2], Ming Liu[2] and He (Helen) Huang[2], *Senior Member, IEEE*

***Abstract*— Existing robotic lower-limb prostheses use autonomous control to address cyclic, locomotive tasks, but are inadequate in adapting to variations in non-cyclic and unpredictable tasks. This study aims to address this challenge by designing a novel electromyography (EMG)-driven musculoskeletal model for volitional control of a robotic ankle-foot prosthesis. The proposed controller ensures continuous control of the device, allowing users to freely manipulate the prosthesis behavior. A Hill-type muscle model was implemented to model a dorsiflexor and a plantarflexor to function around a virtual ankle joint. The model parameters for a subject specific model was determined by fitting the model to the experimental data collected from an able-bodied subject. EMG signals recorded from antagonist muscle pairs were used to activate the virtual muscle models. This model-based approach was then validated via offline simulations and real-time prosthesis control. Additionally, the feasibility of the proposed prosthesis control on assisting the user's functional tasks was demonstrated. The present control may further improve the function of robotic prosthesis for supporting versatile activities in individuals with lower-limb amputations.**

I. Introduction

Lower-limb amputation affects the ability of individuals to perform functional tasks, which severely affects their quality of life [1,2]. These individuals are prescribed passive prostheses which are incapable of restoring much of the biological function of the joint [3]. To overcome this problem, powered prosthesis are being developed with the aim of being lightweight, and generating similar torque and power as that of an able-bodied joints [3-7]. These devices generally use a finite state controller where the task being performed is divided into various states and the device performs a prefixed action when the user is in that state, usually by providing torque or simulating impedance. These controllers are autonomous; meaning they do not incorporate any form of human input into the control algorithm. They rely on the interaction of the device with the environment to identify the user's locomotion state and execute a preprogrammed set of instructions to perform the cyclic locomotion task [6]. Thus, new prosthesis behavior (i.e., not already pre-programmed) cannot be generated by the user to adapt to ever-changing environments (e.g., standing at a crowded bus stop, pushing a lawnmower, playing soccer, etc.) and tasks.

The real world poses many uncertainties present in the environment in the form of terrain variations, obstacles, etc. Such uncertainties require spontaneous responses from the user to adapt to these changes. The lack of active adaptive control of the prosthetic ankle joint leads to poorer stability and balance confidence [8]. This lack of balance confidence and absence of human intent from these autonomous controllers has been a hindrance to these prostheses being used in the real world.

EMG control has seen a lot of popularity recently as a method for volitional control of lower limb prostheses [9]. The addition of human intent to these controllers has the potential to allow amputees to modulate their prosthesis mechanics to react to the uncertainties, and volitionally perform non-repetitive tasks. There are two popular methods that use EMG control: Supervisory EMG control and Direct EMG control. Supervisory control is a form of discrete control where a pattern classifier is used to identify human intent by selecting the appropriate type of locomotion model [10-12]. This type of control requires a significant amount of training data from the user of the device to train the pattern classifiers and is prone to classification errors, which may lead to walking instability in prosthesis users. Continuous EMG control is another method used where the EMG signal is directly related to the force generated by the muscle [13]. This type of continuous volitional control mimics the biological musculoskeletal systems and places the human in direct control making reactionary and non-cyclic tasks possible.

While direct EMG control can restore the ability to adapt to various environments it's unclear whether amputees can coordinate residual muscle activations to reproduce normative ankle joint function. Recent studies have shown that with appropriate training transtibial amputees can regain considerable coordination of voluntary residual muscle activity [14]. These studies have also evaluated the ability of amputee individuals to use this proportional myoelectric control to perform typical daily-life tasks and balancing tasks [14,15]. They implemented proportional myoelectric control on an ankle prosthesis where the muscle behavior was achieved using pneumatic artificial muscles also known as McKibben actuators. The pneumatic actuators modeled muscle behavior while the proportional EMG relayed the human intent to the system. Though this type of control has shown tremendous success, the need for pneumatic actuators that simulate muscle behavior constraints the solution to lab applications.

*Research supported by NSF 1954587 and NIH NICHD F31HD101285
[1]Chinmay Shah is with the Department of Mechanical and Aerospace Engineering at North Carolina State University, USA (cshah@ncsu.edu).

[2]Aaron Fleming, Varun Nalam, Ming Liu and He(Helen) Huang are with the Joint Department of Biomedical Engineering at North Carolina State University and University of North Carolina at Chapel Hill, USA (ajflemin@ncsu.edu, vnalam@ncsu.edu, hhuang11@ncsu.edu)

2022 IEEE/RSJ International Conference on Intelligent Robots and Systems (IROS) | 978-1-6654-7927-1/22/$31.00 ©2022 IEEE | DOI: 10.1109/IROS47612.2022.9981305

The goal of this study was to design a novel EMG-driven musculoskeletal (MSK) model for continuous volitional control of robotic ankle prosthesis. While MSK model-based controllers have been applied to lower limb prosthesis control previously, these virtual muscle models capture the adaptability of the muscle to generate force depending on the state of the muscle but lack volitional (or EMG) control from the user. These studies have shown the capability of MSK model-based controllers to adapt to walking speeds, incline decline walking [16], and also stair climbing and stair descent [17]. Though these MSK controllers are more adaptable than other autonomous controllers, they are limited to locomotion tasks only. EMG-driven MSK model has been successfully implemented in upper-limb prosthesis control [18,19]. However, we are unaware of an EMG-driven MSK controller for motorized lower-limb prosthesis control. Therefore, this study made the following contribution to the field. 1) We developed a novel EMG-driven MSK model to determine the ankle joint torque based on EMG signals from the *tibialis anterior (TA)* and the *gastrocnemius (GAS).* 2) For the first time, this type of EMG-driven control approach was successfully implemented on lower limb wearable robots through a motorized robotic ankle prosthesis. 3) We showed the feasibility of our proposed control to assist with daily activities that did not include cyclic, predictive motion of the ankle.

II. Methodology

In this paper, we propose an EMG-driven MSK model-based controller where we use the EMG from the *TA* and *GAS* to activate a pair of antagonistic virtual muscles of a simplified MSK ankle model. While several muscles contribute to the ankle flexion moment in the sagittal plane, developing a model that includes all muscles would lead to a highly complex model, requiring many parameters and multiple EMG inputs [18]. Thus, we modeled the virtual muscles as a lumped parameter model, where one muscle was used to represent the combined effect of multiple muscles responsible for generating the required force. We used this virtual muscle model combined with the musculoskeletal geometry to predict the ankle joint torque. During real-time control, this predicted ankle torque was sent as the reference torque command to the *VSeM* robotic ankle prosthesis [20]. Fig. 1 depicts the control layout with the important parts of the EMG-driven MSK model, A. Activation Dynamics B. Musculoskeletal Geometry, and C. Muscle Contraction Dynamics.

A. Activation Dynamics (EMG to Muscle Activation)

For real-time control, we placed EMG electrodes (Motion Lab Systems, MA 400) on the *TA* and *GAS*. We high pass filtered (cutoff at 40Hz, 4th Order Butterworth) to get rid of any motion artifacts. We then rectified the signal before implementing a moving average function with a 100ms sliding window to develop the EMG envelope. The 100ms sliding window was determined empirically to optimize performance without introducing considerable amount of delay in the system. We then normalized the resulting signal using the signal value at maximum voluntary contraction (MVC) of each muscle. The MVC is obtained at the beginning of the trial by averaging the signal obtained from three voluntary contraction attempts.

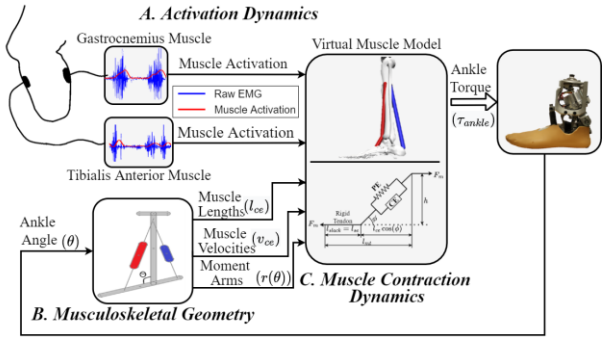

Figure 1. EMG-driven MSK model-based controller layout and model components - A. Activation Dynamics (EMG to muscle activation), B. Musculoskeletal Geometry and, C. Muscle Contraction Dynamics.

We used this rectified, normalized, and enveloped EMG ($e(t)$) signal to calculate the corresponding neural activation ($u(t)$), using a discrete version of a second-order differential equation used to represent the relation between EMG and neural activation [21],

$$u(t) = \alpha\, e(t-d) - \beta_1\, u(t-1) - \beta_2\, u(t-2) \qquad (1)$$

where $\alpha = 0.9486$, $\beta_1 = -0.056$ & $\beta_2 = 0.000627$ [22]. d represents the electromechanical delay present between the onset of the EMG signal and the contraction of the muscle to generate force. This delay was determined based on the experimental data collected for the training of the model and further tuned for real-time control corresponding to the delay present in the robotic ankle prosthesis. At lower levels of force, this neural activation has a non-linear relationship with muscle activation. This relationship was captured through eq.2 [22].

$$a(t) = \frac{e^{Au(t)} - 1}{e^{A} - 1} \qquad (2)$$

where A represents the non-linear shape factor, which is constrained between, $-3 < A < 0$. $a(t)$ represents the final input that was sent to the virtual muscle model as muscle activation.

B. Musculoskeletal Geometry

The musculoskeletal geometry defines how the muscle attaches to the skeleton. It is used to capture the relationship between the change in length of the moment arm with the change in joint angle. The joint torque produced is the product of the muscle force and the moment arm, $\tau_m = r(\theta)F_m$. The moment arm r is a function of joint angle (θ) and this relation was given by the following equation [23].

$$r(\theta) = r_{max}\, cos(\theta - \theta_{max}) \qquad (3)$$

where r_{max} is the maximum moment arm length and θ_{max} is the angle at which, the moment arm is maximum in length. θ is the ankle joint angle measured between the shank and the foot. This angle was measured using the encoder built into the ankle prosthesis when the control was implemented in real-time on the robotic ankle prosthesis. The length of the muscle unit is also a function of the joint angle, it was computed using the following relation [23].

$$l_{mt} = l_o \cos(\phi_{ref}) + l_{slack} - r\sin(\theta_{max} - \theta_{ref}) + r\sin(\theta_{max} - \theta) \quad (4)$$

where l_{mt} is the length of the muscle unit, which is defined as the length of the entire muscle between the attachment points. l_o is the optimal muscle fiber length, which is the length of the muscle fiber when the muscle generates peak force. l_{slack} represents the slack length of the tendon unit in the muscle model. θ_{ref}, ϕ_{ref} are the ankle angle and pennation angle respectively, when the muscle fiber length (l_{ce}) is equal to the optimal muscle fiber length (l_o).

The length of the muscle model can also be expressed as the sum of contractile element length (muscle fiber length) and series elastic element(tendon) length.

$$l_{mt} = l_{ce}\cos(\phi) + l_{se} \quad (5)$$

Since a rigid tendon model was assumed, the length of the tendon/series elastic element does not change i.e., $l_{slack} = l_{se}$. This affects the accuracy of the model but helps to reduce the complexity of the problem [24].

$$\phi(t) = sin^{-1}\left(\frac{l_o \sin(\phi_{ref})}{l_{ce}}\right) \quad (6)$$

The pennation angle, ϕ, changes with the length of the muscle unit and is evaluated using eq. 6 by assuming that the muscle fibers maintain a constant thickness and volume during muscle contraction was made [19].

Eq 4, 5, and 6 and their derivatives were used to compute $length$ of the contractile element (l_{ce}) and velocity of contraction (v_{ce}), which are the inputs sent to the muscle model for calculating the corresponding muscle force.

C. Muscle Contraction Dynamics

The Hill-type muscle model consists of an active contractile element (responsible for generating the force), a parallel passive element, and a series elastic element (tendon). As a rigid tendon assumption was made, the series elastic element was not included in the model. The force generated by the muscle model F_m was given by

$$F_m = (F_{ce} + F_{pe})\cos(\phi) \quad (7)$$

where F_{ce} represents the force generated by the contractile element and F_{pe} denotes the force generated by the parallel elastic element. F_{ce} is a function of l_{ce}, v_{ce} and a which represent the length of the contractile element, the velocity of contraction, and muscle activation respectively.

$$F_{ce} = F_{max}F_l(l_{ce})F_v(v_{ce})a \quad (8)$$

F_{max} here represents the maximum isometric force generated by the muscle. $F_l(l_{ce})$& $F_v(v_{ce})$represent the force-length and force-velocity relationship for a Hill-type muscle model, which are defined as [25],

$$F_l(l_{ce}) = e^{\frac{-(l_o - l_{ce})^2}{(l_o w)^2}} \quad (9)$$

$$F_v(v_{ce}) = \begin{cases} \dfrac{v_{max} - v_{ce}}{v_{max} + Kv_{ce}}, v_{ce} < 0 \\ N + (N-1)\dfrac{v_{max} + v_{ce}}{7.56Kv_{ce} - v_{max}}, v_{ce} \geq 0 \end{cases} \quad (10)$$

w was fixed to a value of 0.56 [25], this parameter adjusts the width of the bell-shaped curve representing the force-length behavior of the muscle model. In Eq 9. v_{max} represents the maximum contraction velocity of the muscle fiber which was set to 10 l_o/s [26,27]. K is the shape parameter fixed to 5 [25] and N is a dimensionless force constant fixed at 1.5 [25]. v_{max}, K and N are fixed constants that govern the dynamic force-length and force-velocity relations of the muscle. The parallel elastic element present in the system only contributes to force generation if the muscle fibers are stretched beyond the optimal fiber length l_o [25].

$$F_{pe} = F_{max}\left(\frac{l_{ce} - l_o}{l_o \epsilon_{pe}}\right)^2, l_{ce} > l_o \quad (11)$$

In Eq 11. ϵ_{pe} is the reference strain which is fixed at 0.56 [25]. Combining all of the equations, the net ankle joint torque was computed by summing the torque contribution of the 2 muscles present in the model,

$$\tau_{ankle} = F_{m(dorsi)}r_{dorsi}(\theta) - F_{m(plant)}r_{plant}(\theta) \quad (12)$$

where τ_{ankle} represents the model predicted ankle torque. This model predicted torque was sent as the reference torque/commanded torque to the robotic ankle prosthesis.

D. Model Parameter Optimization

The EMG-driven MSK model consists of many parameters that allow it to replicate the dynamic force-generating behavior of muscles. While some parameters are fixed to preserve this dynamic relationship, some parameters are responsible for scaling the muscle force according to a specific muscle in the body. The optimization problem was set up to find a set of parameters that would allow the muscle model predictions to best fit the biological ankle torque collected during walking tasks. F_{max}, l_o, r_{max}, θ_{ref}, θ_{max} were the physiological parameters chosen for optimization. θ_{ref} and θ_{max} values were shared by both the muscles; where their function was interchanged i.e., θ_{ref} for dorsiflexor muscle was equal to θ_{max} of the plantar flexor muscle and vice versa. This was done to account for the orientation of the muscles and to reduce the total number of parameters chosen for optimization.

TABLE I. NUMERICAL OPTIMIZATION CONSTRAINTS AND OPTIMIZED PARAMETER VALUE

Model Parameter	*Min Value*	*Max Value*	*Fitted Value*
	Plantar flexor		
F_{max} *(N)*	500	6000	4800
l_o *(m)*	0.02	0.06	0.0402
r_{max}*(m)*	0.01	0.065	0.0375
θ_{ref} *(deg)*	60	130	70
θ_{max}*(deg)*	70	130	112
	Dorsi flexor		
F_{max} *(N)*	500	4000	1800
l_o *(m)*	0.02	0.145	0.065
r_{max} *(m)*	0.01	0.065	0.0449

MATLAB's built-in *GlobalSearch* function was recruited to perform the optimization [18]. The goal of this optimization was to minimize the sum of squared error between the model predicted ankle torque τ_{ankle} and biological ankle torque τ_{bio}, where the error was given by,

$$error = \frac{1}{n}\sum_{1}^{n}(\tau_{ankle} - \tau_{bio})^2 \quad (13)$$

Where n is the length of data used in optimization. Table I. depicts the allowable range of the parameters for optimization and the parameter values obtained after optimization.

E. Evaluation Protocol

We recruited one able-bodied participant (175cm height and 75kg weight) for the study with IRB approval and signed informed consent. To build and validate a subject-specific model, bipolar EMG electrodes were placed on the *TA* and *GAS*. The muscles were located by palpation and visualizing the EMG signal before the data collection. To capture the kinematics of the subject, retroreflective markers were placed on the subject. A 12-camera motion capture system (Vicon, UK) was used to track the marker positions at 100 Hz. The ground reaction forces were measured at 1000 Hz using a split-belt instrumented treadmill (Bertec, USA). The participant was asked to perform various tasks such as walking on the treadmill at 1.0m/s, 1.2m/s, and 1.4m/s, squatting, standing on their toes, and performing sit-to-stand transitions in a non-cyclic or non-periodic manner during data collection. Inverse dynamics were performed using the collected data to calculate the torque generated at the ankle joint when these tasks were performed. EMG signals, ankle angle, and the calculated ankle torque during the walking tasks were used to establish the MSK model parameters via optimization as discussed in the previous section.

Evaluation of our proposed EMG-driven MSK model control included three parts. In the first part, we conducted an offline evaluation of the EMG-driven MSK model for predicting the ankle joint torque. Separate trial data was used in development and evaluation of the model. Next, the EMG-driven model-based controller was validated in real-world scenario using an able-bodied human participant. The human ankle was attached to an able-bodied adaptor to allow able-bodied subjects to wear and operate the device (as shown in the attached supplementary video). Due to the motion constraints imposed by the adaptor, the EMG signals were recorded from the intact side to provide a better representation of muscle activation during functional tasks. This restricted testing of the controller to bilaterally symmetrical tasks. In the second part of the evaluation, we tested the model-based control in an open loop with non-weight bearing posture tasks. The subject sat on a chair comfortably and performed ankle dorsiflexion and plantarflexion repeatedly on the intact limb in a random noncyclic manner. The EMG-driven MSK model estimated the intact ankle torque and then applied it to the prosthetic ankle. In the third part of the evaluation, we aimed to show the feasibility of our proposed control in a closed-loop (with a human operator in the loop), using weight-bearing tasks. The tasks included standing on toes and performing sit-to-stand transitions. Data collected during these real-time evaluations was recorded at 1000 Hz. The prosthesis-generated ankle torque was measured using a loadcell present in the ankle prosthesis [20].

H. Data Analysis and Evaluation Metrics

The optimization was performed in MATLAB (Mathworks, Natick, MA). Biological ankle torque was calculated using the kinematic joint motion and ground reaction forces using an inverse dynamic model. Visual 3D (C-motion Inc., USA) was used to perform the inverse dynamics calculations.

In the first part of the evaluation, we used R^2 and Normalized Root Mean Square Error (NRMSE) values between inverse-dynamic calculated biological ankle torque and model predicted ankle torque to assess the accuracy of the MSK model. Since all the tested tasks were repeated motions, we segmented each repetition, normalized the duration of each repetition as % completion of each attempt, and averaged all the repetitions across the same task. In the second and third parts of the evaluation, NRMSE and R^2 values were calculated between the model predicted ankle torque, the ankle angle/torque of the prosthesis, and biological ankle angle/torque on the intact side.

III. Results And Discussion

A. Offline Simulations

Fig 2. compares the ankle torque predicted by the EMG-driven MSK (blue dashed line) and the biological ankle torque calculated by the inverse dynamics (red solid line) for various tasks. Table II. lists the NRMSE and R^2 values between measured and predicted ankle torque.

For walking at different speeds (1.0m/s and 1.4m/s) and sit-to-stand transitions we observed similar results between our offline analysis and biological ankle torque (Fig 2 A., B. C.). The prediction accuracy in the case of standing on toes and squatting was relatively low which can be seen from Fig 2 D. & E. and the R^2 and NRMSE values in Table II. This reduced prediction accuracy in some tasks might be because the model was trained on the experimental data collected during the walking task and it couldn't adapt very well to different tasks that have a different range of motion and torque requirements.

B. Real-Time Open-Loop Control in Non-Weight Bearing Posture Task

When the MSK model is used to control prosthesis in an open loop, in general, the robotic prosthesis ankle angle can follow the intact joint angle (Fig. 3C.). Both motions showed qualitative agreement without the presence of significant delay between the prosthesis side movement and intact side.

TABLE II. Ankle torque prediction accuracy during offline simulations via EMG-driven MSK model.

Task	*NRMSE*	R^2
Walking 1m/s	0.1173	0.8210
Walking 1.4 m/s	0.0935	0.8895
Sit to stand	0.1695	0.7792
Standing on Toes	0.1656	0.6842
Squatting	0.1882	0.6205

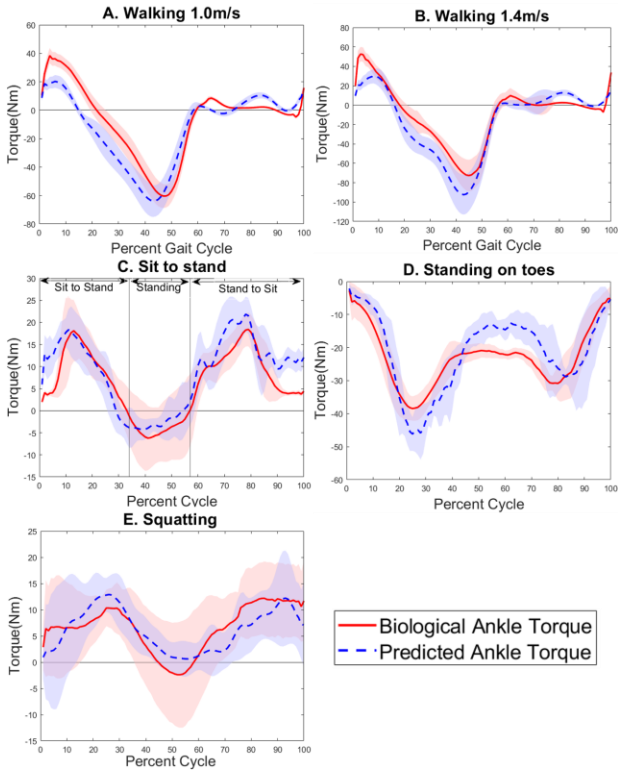

Figure 2. Comparison of the biological ankle torque calculated by inverse dynamics (+ve torque corresponds to dorsiflexion torque and -ve torque represents the plantarflexion torque) with MSK model predicted torque for different tasks: A. walking at 1.0 m/s, B. walking at 1.4 m/s, C. sit-to-stand transitions, D. standing on toes, E. squatting. The solid and dash data represent the averaged curve across multiple repetitions. Shaded area denotes +/- one standard deviation.

(R^2 0.7749 NRMSE 0.1935). The range of motion of the device, however, was lower than the intact side (Fig 3C.). This was due to the limitations of the device used in testing. This control is capable of allowing the user to freely manipulate the ankle position. This is a particularly useful ability that can allow the users to adjust the ankle angle according to the environment, potentially allowing for better obstacle avoidance, sitting posture, terrain adaptation, etc.

C. Real-Time Closed-loop Control in Weight-Bearing Symmetric Tasks

The two tasks that were chosen were - Standing on toes and sit-to-stand transitions. Fig -4 and Fig-5 depict the real-time performance of the control when tasks were performed. Table III. compares the NRMSE and R^2 values for averaged torque and angles values for the different conditions tested.

Sit-to-stand transitions and standing on toes were tested as they are volitional, non-repetitive tasks, that other autonomous controllers cannot perform or assist with. The model predicted torque showed a high correlation with the intact side torque and the torque generated by the prosthesis, which can be seen in Table III (Real-time control with the device is shown in the attached supplementary video). Interestingly, in both cases, the accuracy of the MSK model in ankle torque prediction here was higher than the accuracy shown in offline analysis (Table II). Though EMG signals used to generate prosthetic ankle torque were obtained from the intact limb, the improvement in accuracy may be a result

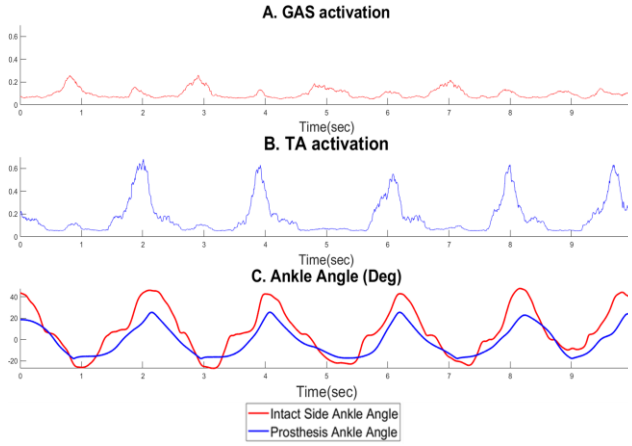

Figure 3. Real-time performance of EMG-driven MSK model-based control in open loop. *A*: Muscle activation of *GAS* on the intact side; *B:* Muscle activation of *TA* on the intact side. They were the inputs of the control. *C*: Prosthesis ankle angle was the output of the control. It was compared to the intact ankle angle (+ve values-dorsiflexion and -ve values-plantarflexion).

of differences between intact and prosthetic limb states (i.e., the joint angles were not identical). In the future, we plan to shift testing with amputee subjects where their residual muscles will be used to drive the robotic prosthetic ankle torque. In that case, even though the model estimation has errors, the human operator can modify the muscle contraction to meet the task goal.

IV. Conclusion

In this study, we developed a novel EMG-driven MSK model-based controller for real-time control of a motorized, robotic ankle prosthesis. The model prediction accuracy was evaluated through offline simulations, where the model predicted torque was compared with the biological ankle torque, computed via inverse dynamics. The EMG-driven MSK model was also implemented for the first time on a robotic ankle prosthesis and evaluated online. The results showed that the personalized MSK model can accurately

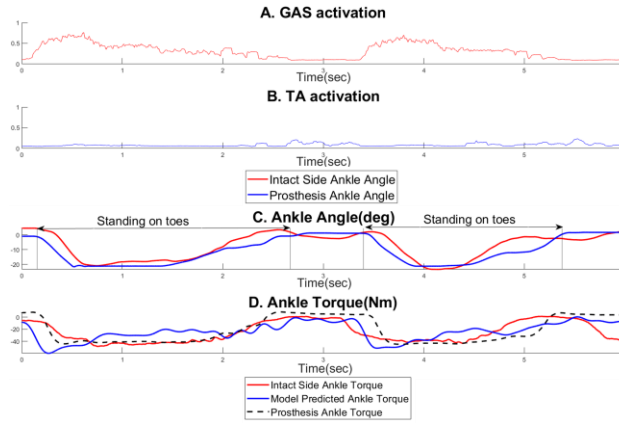

Figure 4. Real-time performance for Standing on toes task. A. and B. Muscle activation for *GAS* and *TA* muscles, respectively. C. Comparison of the ankle angle for the intact and prosthetic side (+ve values – dorsiflexion, -ve values – plantarflexion). D. Comparison of ankle torque of the intact side, the model predicted torque and the torque generated by the prosthetic ankle. (+ve values – dorsiflexion torque, -ve values – plantarflexion torque).

predict the ankle joint torque in various task contexts based on the activity of antagonistic ankle muscles. In addition, for the first time, we showed the feasibility of design of robotic ankle control based on biomimicry principles to enable the performance of prosthesis users on tasks that are unpredictable and non-cyclic. This study also had limitations. As the evaluation was performed with an able-bodied subject using the able-bodied adaptor, the real-time tests were restricted to only bilaterally symmetric tasks. Our future efforts will focus on testing the proposed control on individuals with transtibial amputations when performing functional activities in daily living.

ACKNOWLEDGMENT

The authors would like to thank Wentao Liu, and Sameer Upadhye for their support in this work.

REFERENCES

[1] K. Hagberg and R. Brånemark, "Consequences of non-vascular trans-femoral amputation: a survey of quality of life, prosthetic use and problems," (in eng), *Prosthet Orthot Int,* vol. 25, no. 3, pp. 186-94, Dec 2001, doi: 10.1080/03093640108726601.

[2] M. W. Legro *et al.*, "Issues of importance reported by persons with lower limb amputations and prostheses," (in eng), *J Rehabil Res Dev,* vol. 36, no. 3, pp. 155-63, Jul 1999. [Online]. Available: https://www.ncbi.nlm.nih.gov/pubmed/10659798.

[3] M. Goldfarb, "Consideration of Powered Prosthetic Components as They Relate to Microprocessor Knee Systems," *JPO Journal of Prosthetics and Orthotics,* vol. 25, p. P6U P75, 2013.

[4] S. Au, M. Berniker, and H. Herr, "Powered ankle-foot prosthesis to assist level-ground and stair-descent gaits," *Neural Netw,* vol. 21, no. 4, pp. 654-66, May 2008. [Online]. Available: http://www.ncbi.nlm.nih.gov/entrez/query.fcgi?cmd=Retrieve&db=PubMed&dopt=Citation&list_uids=18499394.

[5] F. Sup, H. A. Varol, J. Mitchell, T. J. Withrow, and M. Goldfarb, "Self-Contained Powered Knee and Ankle Prosthesis: Initial Evaluation on a Transfemoral Amputee," (in eng), *IEEE ... International Conference on Rehabilitation Robotics : [proceedings],* vol. 2009, pp. 638-644, 2009, doi: 10.1109/ICORR.2009.5209625.

[6] M. Liu, F. Zhang, P. Datseris, and H. Huang, "Improving Finite State Impedance Control of Active-Transfemoral Prosthesis Using Dempster-Shafer Based State Transition Rules," *Journal of Intelligent & Robotic Systems,* vol. 76, pp. 461-474, 2014.

[7] T. Lenzi, M. Cempini, L. Hargrove, and T. Kuiken, "Design, development, and testing of a lightweight hybrid robotic knee prosthesis," *The International Journal of Robotics Research,* vol. 37, no. 8, pp. 953-976, 2018/07/01 2018, doi: 10.1177/0278364918785993.

[8] K. Zhang *et al.*, "A subvision system for enhancing the environmental adaptability of the powered transfemoral prosthesis," *IEEE transactions on cybernetics,* vol. 51, no. 6, pp. 3285-3297, 2020.

[9] A. Fleming, N. Stafford, S. Huang, X. Hu, D. P. Ferris, and H. H. Huang, "Myoelectric control of robotic lower limb prostheses: a review of electromyography interfaces, control paradigms, challenges and future directions," (in eng), *J Neural Eng,* vol. 18, no. 4, Jul 27 2021, doi: 10.1088/1741-2552/ac1176.

[10] H. Huang, T. A. Kuiken, and R. D. Lipschutz, "A strategy for identifying locomotion modes using surface electromyography," (in eng), *IEEE Trans Biomed Eng,* vol. 56, no. 1, pp. 65-73, Jan 2009, doi: 10.1109/tbme.2008.2003293.

[11] H. Huang, F. Zhang, L. J. Hargrove, Z. Dou, D. R. Rogers, and K. B. Englehart, "Continuous locomotion-mode identification for prosthetic legs based on neuromuscular-mechanical fusion," (in eng), *IEEE Trans Biomed Eng,* vol. 58, no. 10, pp. 2867-75, Oct 2011, doi: 10.1109/tbme.2011.2161671.

[12] R. Gupta and R. Agarwal, "Single channel EMG-based continuous terrain identification with simple classifier for lower limb prosthesis," *Biocybernetics and Biomedical Engineering,* vol. 39, no. 3, pp. 775-788, 2019.

[13] K. G. Rabe, T. Lenzi, and N. P. Fey, "Performance of Sonomyographic and Electromyographic Sensing for Continuous Estimation of Joint Torque During Ambulation on Multiple Terrains," *IEEE Transactions on Neural Systems and Rehabilitation Engineering,* vol. 29, pp. 2635-2644, 2021.

[14] A. Fleming, S. Huang, E. Buxton, F. Hodges, and H. H. Huang, "Direct continuous electromyographic control of a powered prosthetic ankle for improved postural control after guided physical training: A case study," *Wearable Technologies,* vol. 2, p. e3, 2021, Art no. e3, doi: 10.1017/wtc.2021.2.

[15] A. Fleming and H. H. Huang, "Proportional Myoelectric Control of a Powered Ankle Prosthesis for Postural Control under Expected Perturbation: A Pilot Study," in *2019 IEEE 16th International Conference on Rehabilitation Robotics (ICORR)*, 24-28 June 2019 2019, pp. 899-904, doi: 10.1109/ICORR.2019.8779509.

[16] M. F. Eilenberg, H. Geyer, and H. Herr, "Control of a powered ankle-foot prosthesis based on a neuromuscular model," (in eng), *IEEE Trans Neural Syst Rehabil Eng,* vol. 18, no. 2, pp. 164-73, Apr 2010, doi: 10.1109/tnsre.2009.2039620.

[17] U. Tahir *et al.*, "Case Study: A Bio-Inspired Control Algorithm for a Robotic Foot-Ankle Prosthesis Provides Adaptive Control of Level Walking and Stair Ascent," (in English), *Frontiers in Robotics and AI,* Original Research vol. 5, no. 36, 2018-April-11 2018, doi: 10.3389/frobt.2018.00036.

[18] D. L. Crouch and H. Huang, "Lumped-parameter electromyogram-driven musculoskeletal hand model: A potential platform for real-time prosthesis control," (in eng), *J Biomech,* vol. 49, no. 16, pp. 3901-3907, Dec 8 2016, doi: 10.1016/j.jbiomech.2016.10.035.

[19] L. Pan, D. L. Crouch, and H. Huang, "Myoelectric Control Based on a Generic Musculoskeletal Model: Toward a Multi-User Neural-Machine Interface," *IEEE Transactions on Neural Systems and Rehabilitation Engineering,* vol. 26, no. 7, pp. 1435-1442, 2018, doi: 10.1109/TNSRE.2018.2838448.

[20] S. Upadhye, C. Shah, M. Liu, G. Buckner, and H. H. Huang, "A Powered Prosthetic Ankle Designed for Task Variability - A Concept Validation," presented at the International Conference on Intelligent Robots and Systems, Prague, 2021.

[21] T. S. Buchanan, D. G. Lloyd, K. Manal, and T. F. Besier, "Neuromusculoskeletal modeling: estimation of muscle forces and joint moments and movements from measurements of neural command," (in eng), *Journal of applied biomechanics,* vol. 20, no. 4, pp. 367-395, 2004, doi: 10.1123/jab.20.4.367.

[22] D. G. Lloyd and T. F. Besier, "An EMG-driven musculoskeletal model to estimate muscle forces and knee joint moments in vivo," (in eng), *J Biomech,* vol. 36, no. 6, pp. 765-76, Jun 2003, doi: 10.1016/s0021-9290(03)00010-1.

[23] H. Geyer and H. Herr, "A muscle-reflex model that encodes principles of legged mechanics produces human walking dynamics and muscle activities," (in eng), *IEEE Trans Neural Syst Rehabil Eng,* vol. 18, no. 3, pp. 263-73, Jun 2010, doi: 10.1109/tnsre.2010.2047592.

[24] M. Millard, T. Uchida, A. Seth, and S. L. Delp, "Flexing computational muscle: modeling and simulation of musculotendon dynamics," (in eng), *J Biomech Eng,* vol. 135, no. 2, p. 021005, Feb 2013, doi: 10.1115/1.4023390.

[25] H. Geyer and A. Seyfarth, "Neuromuscular Control Models of Human Locomotion," in *Humanoid Robotics: A Reference*, A. Goswami and P. Vadakkepat Eds. Dordrecht: Springer Netherlands, 2016, pp. 1-30.

[26] J. M. Winters, "Hill-Based Muscle Models: A Systems Engineering Perspective," in *Multiple Muscle Systems: Biomechanics and Movement Organization*, J. M. Winters and S. L. Y. Woo Eds. New York, NY: Springer New York, 1990, pp. 69-93.

[27] F. E. Zajac, "Muscle and tendon: properties, models, scaling, and application to biomechanics and motor control," (in eng), *Crit Rev Biomed Eng,* vol. 17, no. 4, pp. 359-411, 1989.